Available online at www.sciencedirect.com
SCIENCE DIRECT
Journal of Catalysis 239 (2006) 13–22
JOURNAL OF CATALYSIS
www.elsevier.com/locate/jcat

Theoretical investigation of 1,3-butanediol adsorption on an oxygen-defected $CeO_2(111)$ surface

Naoki Ichikawa [a], Satoshi Sato [b,*], Ryoji Takahashi [b], Toshiaki Sodesawa [b], Harunori Fujita [c], Takashi Atoguchi [c], Akinobu Shiga [d]

[a] *Graduate School of Science and Technology, Chiba University, Yayoi, Inage, Chiba 263-8522, Japan*
[b] *Department of Applied Chemistry, Faculty of Engineering, Chiba University, Yayoi, Inage, Chiba 263-8522, Japan*
[c] *Polymer Laboratory, UBE Industries Ltd., 8-1 Goi-minamikaigan, Ichihara, Chiba 290-0045, Japan*
[d] *LUMMOX Research Lab., 2-18-4-302 Takezono, Tsukuba, Ibaraki 305-0032, Japan*

Received 19 August 2005; revised 12 January 2006; accepted 16 January 2006

Available online 15 February 2006

Abstract

The adsorption of 1,3-butanediol on an oxygen-defect site of a $CeO_2(111)$ surface was investigated with density functional theory (DFT) and paired interacting orbital (PIO) calculations in connection with the investigation of a $CeO_2(111)$ stoichiometric surface. At the oxygen-defect site, two adsorption structures were obtained by DFT calculations. In the structures, the two oxygen atoms of the OH groups interact with exposed Ce cations at the oxygen-defect site. The adsorption structures at the oxygen-defect site are more stable than that on the stoichiometric surface. In the most stable adsorption structure, one hydrogen atom of the 2-position methylene group interacts with the third Ce cation at the oxygen-defect site of the $CeO_2(111)$ surface. We confirmed the elongation of two C–O bonds and one C–H bond of the 2-position methylene group in the most stable adsorption structure. We also executed PIO calculations of 1,3-butanediol-$CeO_2(111)$ systems to analyze interacting orbitals. In-phase interaction between the two oxygen atoms in 1,3-butanediol and Ce cations was observed, indicating that the 1,3-butanediol molecule is anchored by two O–Ce bonds. Out-of-phase interactions between O and C atoms at 1-position and between H and C atoms at 2-position were confirmed.

Keywords: DFT and PIO calculations; CeO_2; 1,3-diol; Unsaturated alcohol

1. Introduction

We recently reported the selective dehydration of 1,3-diols over CeO_2 catalyst to form unsaturated alcohols [1–3]. For example, 1,3-propanediol was dehydrated to form 2-propen-1-ol at 325 °C with 98.9 mol% selectivity, and 1,3-butanediol was dehydrated to form 3-buten-2-ol and *trans*-2-buten-1-ol with 56.9 and 35.5 mol% selectivity, respectively [2]. In the dehydration of 1,3-butanediol, CeO_2 shows structure-sensitive catalysis [3]; the {111} facets have active sites for the formation of unsaturated alcohols, and the other surfaces catalyze such side reactions as the decomposition of 1,3-butanediol. The catalytic performance of CeO_2 in the reaction of 1,3-butanediol is greatly affected by its crystallite size; the selectivity to unsaturated alcohols, such as 3-buten-2-ol, increases with increasing crystallite size, whereas the decomposition of 1,3-butanediol into methanol is catalyzed by small CeO_2 particles. The {111} facets are predominant on large CeO_2 particles, whereas the {100} and {110} facets are exposed on small particles.

We have proposed the following reaction mechanism for the dehydration of 1,3-diols over CeO_2 [2]: Three Ce cations positioned in a manner forming a triangle and exposed at an oxygen-defect site of the $CeO_2(111)$ surface are the active center for the dehydration, and two oxygen atoms of the OH groups and one hydrogen atom of the 2-position methylene group in 1,3-diol interact with the three Ce cations. Then the hydrogen atom is radically abstracted as the initial step, followed by the abstraction of one of the OH groups in 1,3-diol to produce the corresponding unsaturated alcohols.

In a previous paper [4], to prove our proposed reaction mechanism, we performed quantum chemical calculations based on

* Corresponding author.
E-mail address: satoshi@faculty.chiba-u.jp (S. Sato).

0021-9517/$ – see front matter
doi:10.1016/j.jcat.2006.01.017

the paired interacting orbital (PIO) theory in the aforementioned model and confirmed the abstraction process of the hydrogen atom of the 2-position methylene group by a Ce cation. But the adsorption model that we used for our calculations was based on speculation derived from the reaction results, and we did not optimize the adsorption structure. Highly reliable calculations, such as ab initio and density functional theory (DFT) calculations, should be performed.

In this study, we develop the model of the adsorption structure of 1,3-butanediol at an oxygen-defect site of the $CeO_2(111)$ surface, which was optimized with DFT calculations. We also carried out PIO calculations on the stable adsorption structures obtained from DFT calculations, to visualize orbital interactions between 1,3-butanediol and the CeO_2 surface.

2. Calculation methods

2.1. DFT calculations

DFT calculations were performed using the DMol^3 program mounted on MS Modeling 3.0 package [5,6]. Each $CeO_2(111)$ surface model was geometrically optimized at the level of the local density approximation (LDA) using the Vosko–Wilk–Nusair (VWN) functional [7]. The double-numeric polarized (DNP) basis set [5,6], which is equivalent in accuracy to the 6-31G** double-zeta class Gaussian orbital basis set, was also used. Total electronic energy convergence criteria in the geometry optimization were set at 10^{-4} a.u. (1 a.u. = 2625.5 kJ mol^{-1}), and the self-consistent field (SCF) convergence criteria during geometry optimization were set at 10^{-4} a.u. Only the Γ point in the Brillouin zone was sampled. Using the optimized models, single-point electronic energy was calculated at the level of the generalized gradient approximation (GGA) of the Perdew–Burke–Ernzerhof (PBE) functional [8]. DNP basis sets were also used, as in the case of geometry optimization. SCF convergence criteria of GGA electronic calculation were set at 10^{-5} a.u. Brillouin zone integration was performed using a $2 \times 2 \times 1$ Monkhorst–Pack grid [9].

The $CeO_2(111)$ surface model was constructed as a slab-gap model [10]. First, the optimized bulk structure was sliced along

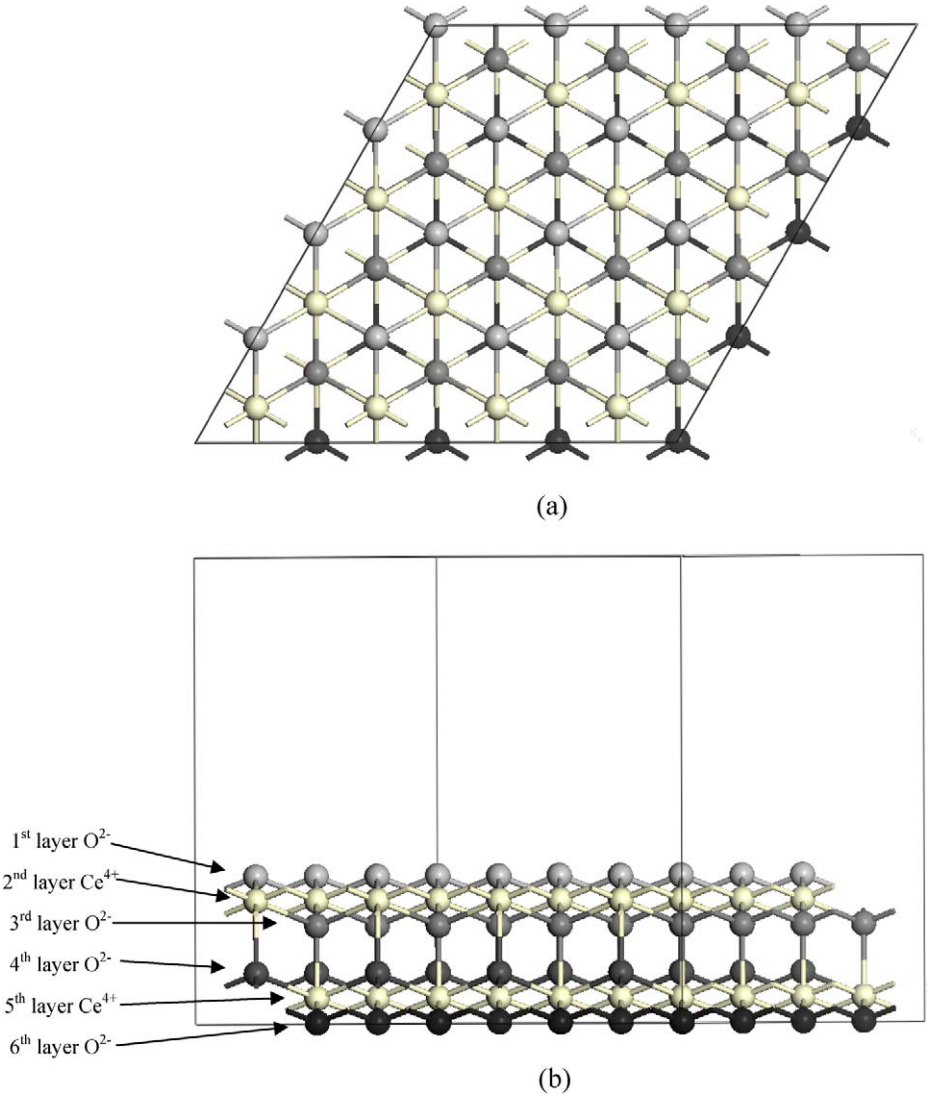

Fig. 1. $CeO_2(111)$ surface before geometry optimization by DFT calculations. (a) Top view, (b) side view.

the specified plane. Then an empty space of adequate height was created along the z-axis, with only two-dimensional periodicity taken into account. Our slab model was six layers thick, and the height of the empty space was set at 10 Å. The lattice parameters of the model, as shown in Fig. 1, were $a = b =$ 15.304 Å, $c = 14.684$ Å, $\alpha = 60.00°$, and $\beta = \gamma = 90.00°$. These parameters were fixed during the subsequent geometry optimization. Fig. 1 shows the structure of the $CeO_2(111)$ surface before geometry optimization by DFT calculations. MOLEKEL 4.0 was used to visualize all results of DFT calculations, except for Fig. 1 [11].

2.2. PIO calculation

The PIO theory of Fujimoto et al. [12,13] was used to analyze orbital interactions between 1,3-butanediol and the $CeO_2(111)$ surface, with optimum geometry obtained by DFT calculations. All PIO calculations were executed with the quantum chemical application software LUMMOX [14], to confirm the interaction between the two substrates and to quantitatively identify the interacting orbitals that played an important role in chemisorption [15–18]. The molecular orbitals were determined on the basis of the extended Hückel theory, using the extended Hückel parameters in the literature [19,20]. The algorithm of the PIO theory is also summarized in the literature [12, 15–18]. The PIO theory quantifies the importance of PIOs between two fragments, A and B; in this study, A is 1,3-butanediol and B is the $CeO_2(111)$ surface. The importance of PIOs is evaluated in terms of eigenvalue (EV). PIOs are labeled as PIO-n, where n indicates the sequence of importance of the PIOs; PIO-1 is the most important PIO, PIO-2 is the second-most important PIO, and so on. The overlap population (OP) is used to evaluate the attractive or repulsive role of the PIO in the adsorption system. PIO with positive OP plays an attractive role in the adsorption, whereas PIO with negative OP plays a repulsive role.

3. Results

Fig. 2 shows the structure of an oxygen defect introduced on the $CeO_2(111)$ surface, which was optimized by DFT calculations. Relaxation of the surface was observed; the third-layer O^{2-} ions around the oxygen defect migrated toward the oxygen-defect site, whereas the second-layer Ce^{4+} ions around the oxygen defect migrated in the opposite direction. No relaxation of the outermost surface O^{2-} ions was observed.

We investigated the adsorption geometry of 1,3-butanediol at an oxygen-defect site of the $CeO_2(111)$ surface. Figs. 3 and 4 show two structures from different starting geometries, which were optimized by the calculations. The nomenclature of the atoms in 1,3-butanediol is shown in Fig. 5. We designate the adsorption models shown in Figs. 3 and 4 as Structures 1 and 2, respectively. In Structure 1, the two oxygen atoms in 1,3-butanediol interact with Ce^1 and Ce^3 cations. In Structure 2, the $H^{2\alpha}$ atom interacts with Ce^2 cation, in addition to the interaction between the two oxygen atoms in 1,3-butanediol and

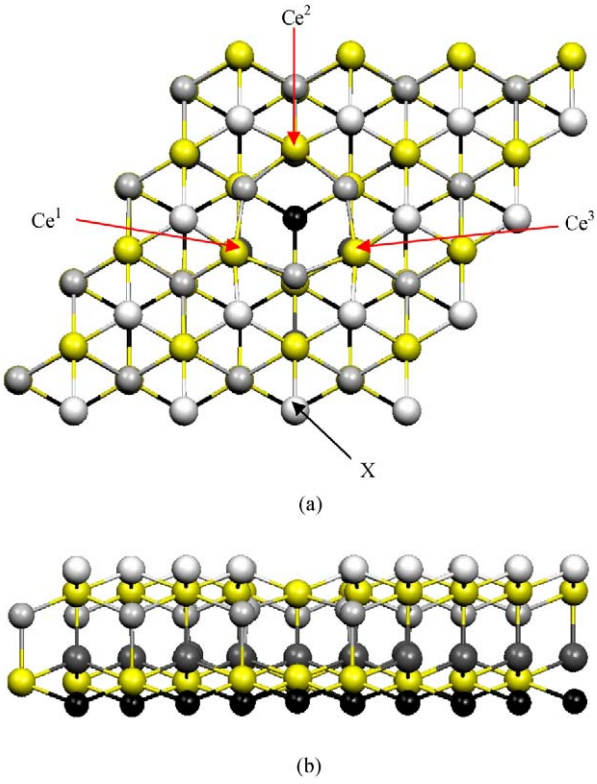

Fig. 2. Structure of $CeO_2(111)$ surface with an oxygen defect optimized by DFT calculations. (a) Top view, (b) side view. In the side view, a first-layer O atom that overlaps with the oxygen-defect site, namely, X in the top view, is removed in order to clearly visualize the oxygen-defect site.

the Ce^1 and Ce^3 cations observed in Structure 1. Another significant difference between the two structures is the molecular structure of 1,3-butanediol: the molecule is linear in Structure 1 and ringed in Structure 2. Table 1 lists the structure parameters of free and adsorbed 1,3-butanediol (Structures 1 and 2). The adsorption energies of 1,3-butanediol at the oxygen-defect site in Structures 1 and 2 are -98.8 and -102.7 kJ mol^{-1}, respectively (Table 2). In Structure 1, an elongation of the C^2–$H^{2\alpha}$ bond by 0.013 Å is observed after the adsorption, whereas no stretching of C–O bonds is observed. In Structure 2, the C^1–O^1 and C^3–O^3 bond lengths are increased together with the elongation of the C^2–$H^{2\alpha}$ bond, whereas the other bond lengths are hardly changed before and after the adsorption.

We built a $(Ce_9O_{36}H_{26})^{12-}$ cluster model from Structure 2 for PIO calculations and defined three cutout planes [(I)–(III), as shown in Fig. 6], to observe the orbital interactions between the two oxygen atoms in 1,3-butanediol and Ce cations, between $H^{2\alpha}$ and Ce^2, and between C^1–O^1 and Ce^1, respectively. Table 3 summarizes EVs, Ops, and LCAO representations of PIOs 1–6, and Fig. 7 shows the contour maps of four representative PIOs. PIO-1 shows in-phase interaction between the oxygen atoms in 1,3-butanediol and Ce cations (Fig. 7a), whereas PIO-5 shows out-of-phase interaction between the atoms (Fig. 7b). PIO-3 exhibits out-of-phase interaction between O^1 and C^1 atoms, which is induced by the in-phase interaction between O^1 and Ce^1 (Fig. 7c). PIO-5 and PIO-6 also exhibited out-of-phase interaction between $H^{2\alpha}$ and C^2, which

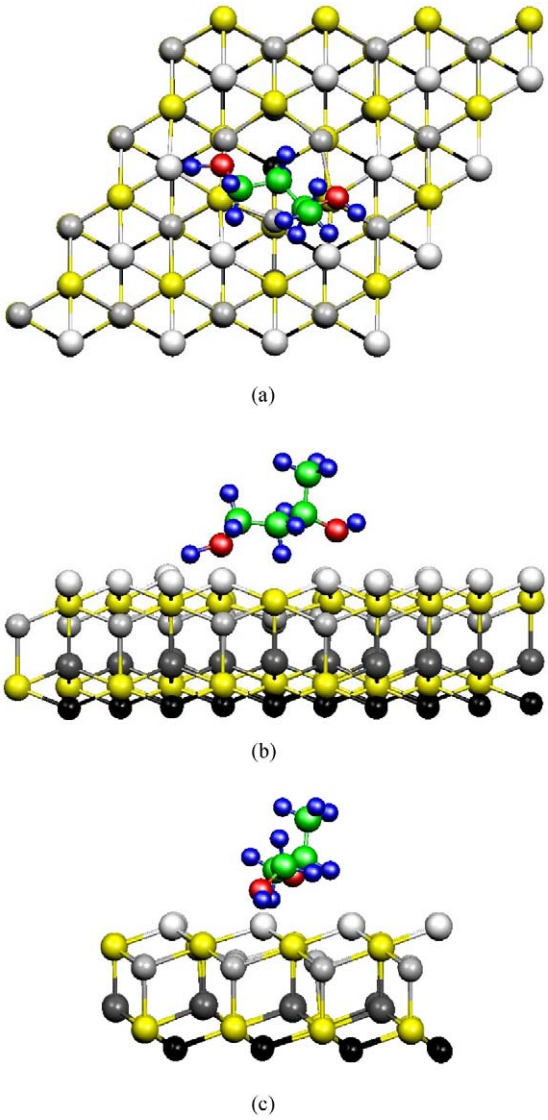

Fig. 3. Optimized structure of 1,3-butanediol at oxygen-defect site of CeO_2 (111) surface (Structure 1). (a) Top view, (b) side view, (c) front view. The O atom, represented by X in Fig. 2, is removed in the side view.

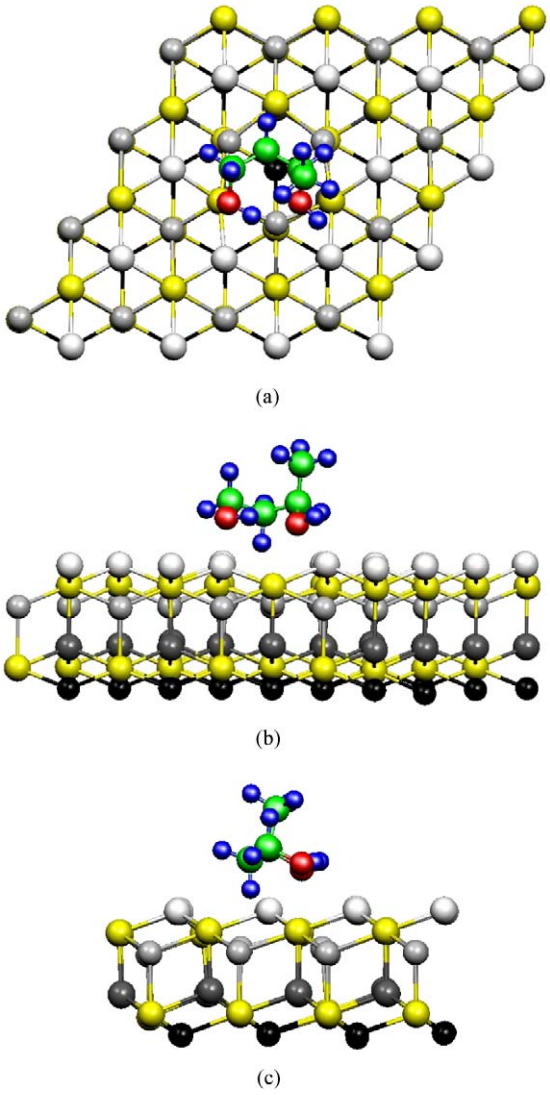

Fig. 4. Optimized structure of 1,3-butanediol at oxygen-defect site of CeO_2 (111) surface (Structure 2). (a) Top view, (b) side view, (c) front view. The O atom, represented by X in Fig. 2, is removed in the side view.

is induced by the in-phase interaction between $H^{2\alpha}$ and Ce^2 (Figs. 7d–7e). In addition, PIO-2, PIO-3, and PIO-4 also exhibited an in-phase interaction similar to PIO-1.

Along with $(Ce_9O_{36}H_{26})^{12-}$, we built other CeO_2 clusters, such as Ce_9O_{18} and $Ce_{20}O_{40}$, with the charge of -2 from Structure 2 (Fig. 4), to confirm the validity of the cluster that we used for the PIO calculations. The calculation results were essentially the same for the three clusters. The 1,3-butanediol molecule is anchored by the interaction between its two oxygen atoms and Ce cations, and an out-of-phase interaction between $H^{2\alpha}$ and C^2, induced by the in-phase interaction between $H^{2\alpha}$ and Ce^2, was observed.

We also investigated the adsorption of 1,3-butanediol on a stoichiometric CeO_2(111) surface. Fig. 8 shows the optimized structure of 1,3-butanediol on the stoichiometric CeO_2(111) surface (Structure 3). Structure 3 has an adsorption energy of -82.7 kJ mol^{-1} (Table 2) and elongated O–H bonds in 1,3-bu-

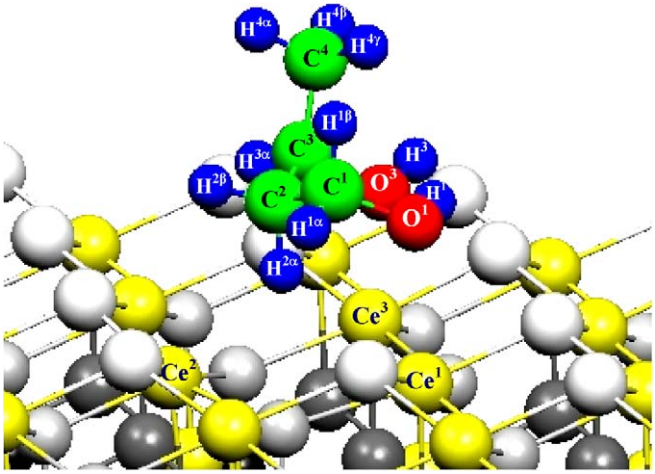

Fig. 5. Perspective view of the adsorption of 1,3-butanediol on oxygen-defect site of CeO_2(111) surface (Structure 2) and nomenclature of the atoms in 1,3-butanediol and three Ce cations.

Table 1
Structure parameters of free and adsorbed 1,3-butanediol molecules together with bond lengths of O^1–Ce^1, O^3–Ce^3 and $H^{2\alpha}$–Ce^{2}[a]

	Bond length[b] (Å)			
	Free	Structure 1	Structure 2	Structure 3
C^1–$H^{1\alpha}$	1.114	1.106	1.104	1.107
C^1–$H^{1\beta}$	1.103	1.117	1.104	1.107
C^1–O^1	1.401	1.400	1.418	1.425
C^2–$H^{2\alpha}$	1.104	1.117	1.113	1.102
C^2–$H^{2\beta}$	1.103	1.104	1.101	1.104
C^3–H^3	1.105	1.108	1.109	1.109
C^3–O^3	1.434	1.424	1.451	1.418
C^4–$H^{4\alpha}$	1.100	1.100	1.102	1.102
C^4–$H^{4\beta}$	1.100	1.101	1.102	1.100
C^4–$H^{4\gamma}$	1.103	1.102	1.102	1.102
O^1–H^{O1}	0.986	1.202	0.986	1.037
O^3–H^{O3}	0.973	0.977	0.984	1.510
O^1–Ce^1	–	2.496	2.565	2.481
O^3–Ce^3	–	2.641	2.673	2.378
$H^{2\alpha}$–Ce^2	–	3.279	2.500	3.194

[a] The nomenclature of each atom is the same as shown in Fig. 5.
[b] Underlined numbers indicate large change in bond length after adsorption.

Table 2
Adsorption energies of 1-butanol, 2-butanol and 1,3-butanediol on oxygen-defected and stoichiometric CeO_2(111) surfaces[a]

Adsorbate	Oxygen-defect site	Stoichiometric surface
1-butanol	−80.1	−64.5
2-butanol	−46.6	−66.2
1,3-butanediol	−98.8, −102.7	−82.7

[a] The unit of energy is kJ mol^{-1}.

tanediol. The structure parameters of Structure 3 are summarized in Table 1.

We also used DFT calculations to investigate the adsorption of 1- and 2-butanol on oxygen-defected and stoichiometric CeO_2(111) surfaces. Table 2 summarizes the adsorption energies of 1- and 2-butanol as well as 1,3-butanediol on the oxygen-defected and stoichiometric CeO_2(111) surfaces. The adsorption energies of the mono-alcohols are lower than those of 1,3-butanediol. Fig. 9 shows the adsorption structures of 1- and 2-butanol at an oxygen-defect site of the CeO_2(111) surface. The butanols are adsorbed to fill the oxygen-defect site with O atoms from the OH groups. In addition, β-H atoms in butanol are located at a distance from Ce cations and thus cannot interact with any Ce cations.

4. Discussion

4.1. Dehydration of 1,3-diols over CeO_2(111) surface

We recently reported that the CeO_2(111) surface serves as the active center for the dehydration of 1,3-diols into unsaturated alcohols [3]. We used CeO_2 catalysts with different crystallite sizes and found that the selectivity to unsaturated alcohols increased with increasing crystallite size. Table 4 gives catalytic data from our earlier study [3] for the reaction of 1,3-butanediol over CeO_2 with different crystallite sizes, along

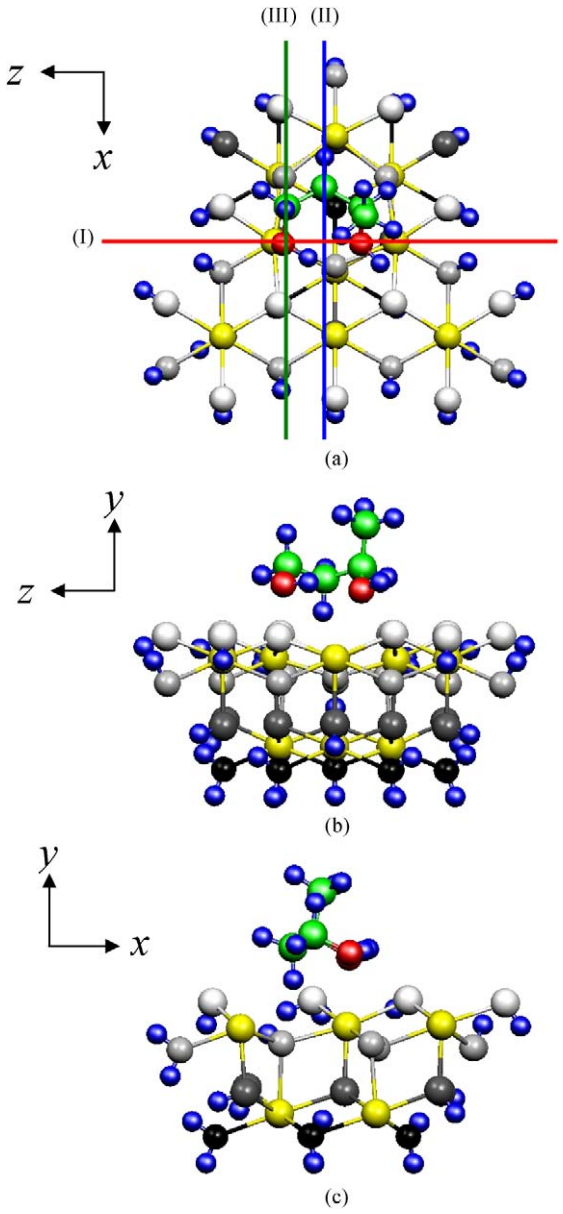

Fig. 6. Graphical images of $Ce_9O_{36}H_{26}$ cluster and 1,3-butanediol for PIO calculations with cut-out planes. (a) Top view, (b) side view, (c) front view. Cut-out planes (I)–(III) were fixed to visualize the cross section of PIOs in Fig. 7, and the $Ce_9O_{36}H_{26}$ cluster and the diol were not cut. The O atom, represented by X in Fig. 2, is removed in the side view.

with the formation rates of unsaturated alcohols calculated using the cited data. The formation rate based on CeO_2 unit surface area monotonically increased with increasing crystallite size (Table 4). We speculate that these results are related to changes in the properties of the CeO_2 surface with crystalline growth. Transmission electron microscopy has revealed that the {111} facets are exposed preferentially on the surface of a large CeO_2 crystallite [21]. The number of surface oxygen defects decreases with increasing crystallite size [22,23]. The oxygen-defected CeO_2(111) single-crystal surface has been observed microscopically [24–28]. A surface oxygen defect exists as a "single vacancy" in the low concentration range of oxygen defects [27,28], with multiple defects of linear and triangular

Table 3
Eigenvalues, overlap populations and LCAO representations of PIO-n ($n = 1$–6)

n	Eigenvalue (EV)	Overlap population (OP)	Component[a]
1	0.863	0.0440	$\psi_1 = -0.151\mathrm{Ce}^1_{5dx2-y2} + 0.137\mathrm{Ce}^1_{5py} + 0.077\mathrm{Ce}^1_{6s} + \cdots$
			$\varphi_1 = -0.682\mathrm{O}^1_{2py} + 0.301\mathrm{O}^1_{2pz} - 0.242\mathrm{O}^3_{2py} - 0.214\mathrm{O}^3_{2pz} - 0.209\mathrm{C}^1_{2pz} + \cdots$
2	0.217	0.0202	$\psi_2 = +0.160\mathrm{Ce}^3_{5dyz} - 0.124\mathrm{Ce}^2_{5dxy} - 0.119\mathrm{Ce}^3_{5dx2-y2} + \cdots$
			$\varphi_2 = -0.426\mathrm{O}^3_{2py} + 0.357\mathrm{C}^2_{2py} - 0.349\mathrm{O}^1_{2px} + 0.278\mathrm{H}^{2\beta}_{1s} - 0.264\mathrm{O}^1_{2pz} + \cdots$
3	0.097	0.0062	$\psi_3 = +0.207\mathrm{Ce}^3_{5py} - 0.143\mathrm{Ce}^1_{5py} - 0.108\mathrm{Ce}^3_{5dyz} + \cdots$
			$\varphi_3 = +0.315\mathrm{C}^3_{2py} - 0.299\mathrm{C}^4_{2py} - 0.214\mathrm{C}^1_{2py} + 0.214\mathrm{O}^1_{2py} - 0.178\mathrm{O}^3_{2pz} + \cdots$
4	0.083	0.0249	$\psi_4 = -0.210\mathrm{Ce}^3_{5dyz} + 0.185\mathrm{Ce}^3_{5dx2-y2} + 0.106\mathrm{Ce}^1_{5py} + \cdots$
			$\varphi_4 = +0.698\mathrm{O}^3_{2py} - 0.353\mathrm{O}^1_{2py} + 0.266\mathrm{O}^3_{2pz} - 0.199\mathrm{O}^1_{2px} + 0.172\mathrm{C}^3_{2px} + \cdots$
5	0.032	−0.0409	$\psi_5 = -0.430\mathrm{Ce}^1_{5py} - 0.309\mathrm{Ce}^1_{6s} - 0.232\mathrm{Ce}^2_{5py} - 0.195\mathrm{Ce}^2_{6s} - 0.174\mathrm{Ce}^2_{5px} + \cdots$
			$\varphi_5 = -0.363\mathrm{C}^1_{2py} + 0.288\mathrm{C}^2_{2s} - 0.276\mathrm{O}^1_{2py} + 0.224\mathrm{O}^1_{2s} - 0.128\mathrm{H}^{2\alpha}_{1s} + \cdots$
6	0.024	0.0199	$\psi_6 = +0.389\mathrm{Ce}^1_{5py} + 0.353\mathrm{Ce}^1_{5dx2-y2} - 0.272\mathrm{Ce}^1_{6s} - 0.104\mathrm{Ce}^2_{5px} - 0.100\mathrm{Ce}^2_{5py} + \cdots$
			$\varphi_6 = -0.344\mathrm{O}^1_{2pz} - 0.272\mathrm{O}^1_{2s} + 0.208\mathrm{C}^2_{2s} + 0.181\mathrm{C}^2_{2px} - 0.150\mathrm{H}^{2\alpha}_{1s} + \cdots$

[a] ψ and φ represent molecular orbitals of $(\mathrm{Ce_9O_{36}H_{26}})^{12-}$ cluster and 1,3-butanediol, respectively.

forms observed only rarely on the surface at a defect concentration of $<1 \times 10^{13}$ cm^{-2} [27].

We speculate that a Ce^{4+} ion at a single defect site acts as the active center for the abstraction of β-H from 1,3-diol via the Ce^{4+}–Ce^{3+} redox cycle [2]. This leads to the following question: Are the multiple defects of linear and triangular forms active centers for the dehydration? Small CeO_2 particles decompose 1,3-butanediol into methano1 and ethanol [3] and contain many defects that would form multiple defects [27]; however, these multiple defects would expose reduced Ce^{3+} ions [26] that would not participate in the redox cycle. Thus, the multiple defects would catalyze the decomposition, not the dehydration, of 1,3-diol.

We have another question: Can the oxygen-defect site exist under the reaction conditions? It has been reported that CeO_2 by nature has oxygen defects, and that the concentration of the oxygen defects depends on its crystallite size [22, 23]. Kosacki et al. indicated that the concentration of oxygen defects decreases with CeO_2 crystalline growth because of the increase in the enthalpy for oxygen-defect formation with growth [22]. Thus, it is reasonable that single oxygen-defect sites exist predominantly on the surface of the most selective CeO_2 at the reaction temperature. Therefore, we considered $CeO_2(111)$ with either a single vacancy or a stoichiometric surface for the investigation of active sites in the dehydration of 1,3-butanediol.

4.2. Structure of the $CeO_2(111)$ surface with oxygen defect

The optimized structure of the oxygen-defected $CeO_2(111)$ surface shows slight relaxation (Fig. 2); the third-layer O anions migrate toward the oxygen-defect direction, whereas the second-layer Ce cations migrate in the opposite direction. In our calculations, relaxation of the first-layer O anions occurred rarely. Using DFT calculations, Esch et al. recently showed relaxation of the oxygen-defected $CeO_2(111)$ surface and confirmed relaxation of the second-layer cations and the third-layer anions, similar to what we found. They also verified that the first-layer O anions relaxed outward, in good agreement with previous experimental results [26–28]. The difference between the results of Esch et al. and our findings can be attributed to the different calculation conditions, the lenient convergence criteria used in our study, and the Hubbard-U term addition used in their study to consider the strong correlation effect [28–30].

4.3. Adsorption of 1,3-butanediol on oxygen-defect site of $CeO_2(111)$ surface

We obtained two adsorption models of 1,3-butanediol on an oxygen-defect site of a $CeO_2(111)$ surface (Figs. 3 and 4). The adsorption energy of Structure 2 (Fig. 4) is larger than that of Structure 1 (Fig. 3) by 3.9 kJ mol^{-1}, indicating that 1,3-butanediol adsorbs on the oxygen-defect site of the $CeO_2(111)$ surface in the form of Structure 2. Comparing the structure parameters of the free molecule of 1,3-butanediol and Structure 2 shows that the C^1–O^1, C^2–$H^{2\alpha}$, and C^3–O^3 bond lengths are increased by 0.009–0.017 Å (Table 1). In the reaction of 1,3-butanediol over CeO_2, 3-buten-2-ol and *trans*-2-buten-1-ol are selectively produced, with the sum of their selectivities >90 mol% [2], and a C^2–$H^{2\alpha}$ bond and one of the C–O bonds must be activated to produce the corresponding unsaturated alcohols. Hence, the elongation of these bonds suggests that the three bonds are activated and that the oxygen defect on the $CeO_2(111)$ surface is an active center for the selective dehydration of 1,3-diols to form unsaturated alcohols. Furthermore, we note that the O^1–Ce^1 bond length is shorter than the O^3–Ce^3 bond length, accounting for the difference in selectivity to 3-buten-2-ol of 56.9 mol% and to *trans*-2-buten-1-ol of 35.5 mol% [2]. 3-Buten-2-ol and *trans*-2-buten-1-ol are formed by the abstraction of an OH group at 1-position and 3-position in 1,3-butanediol, respectively. The

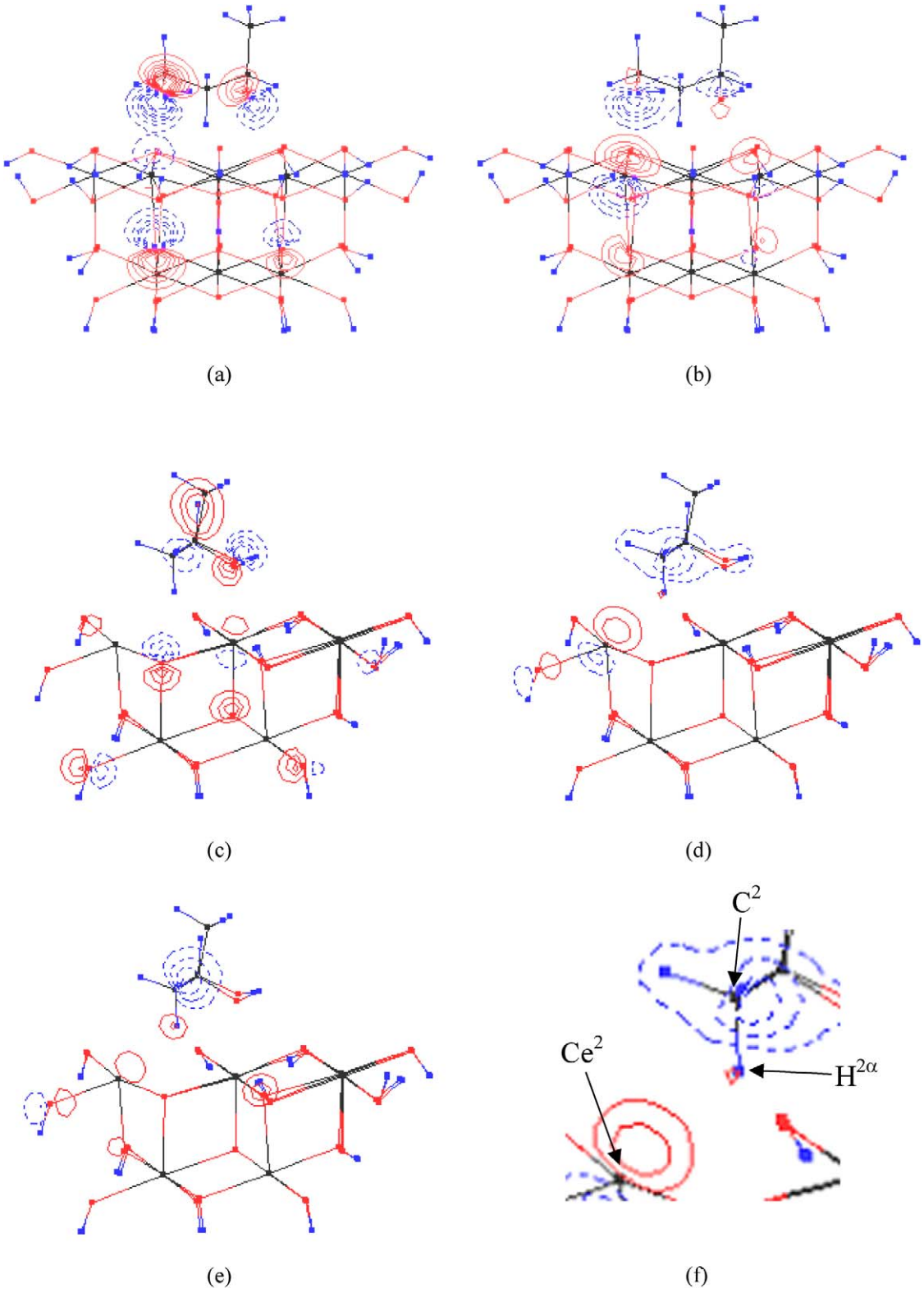

Fig. 7. Contour maps of PIOs. (a) PIO-1 from cut-out plane (I), (b) PIO-5 from (I), (c) PIO-3 from (III), (d) PIO-5 from (II), (e) PIO-6 from (II), (f) expanded image of PIO-5 (d).

OH group at 1-position interacts strongly with the Ce cation, because the O^1 atom is positioned more closely to the Ce cation than the O^3 atom is. Thus, the OH group at 1-position is readily abstracted compared with the OH group at 3-position.

4.4. Orbital interactions between 1,3-butanediol and the CeO_2(111) surface

We performed PIO calculations to investigate the orbital interactions between 1,3-butanediol and the CeO_2(111) surface.

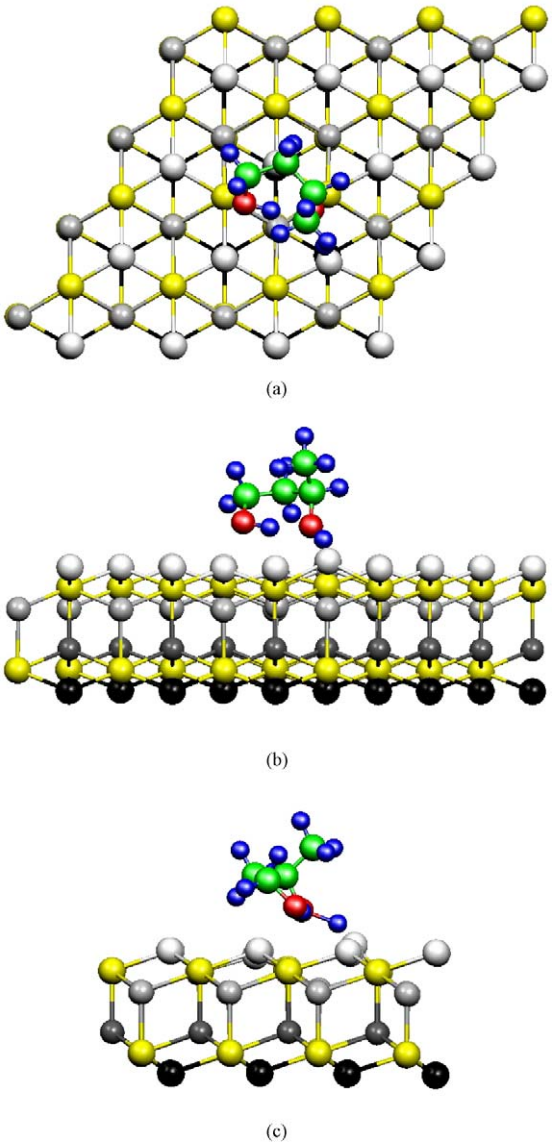

Fig. 8. Adsorption of 1,3-butanediol on stoichiometric $CeO_2(111)$ surface optimized by DFT calculations (Structure 3). (a) Top view, (b) side view, (c) front view.

Fig. 6 shows the $(Ce_9O_{36}H_{26})^{12-}$ cluster-1,3-butanediol adsorption structure modeled from Structure 2 for the PIO calculations. As is well known, two Ce^{4+} ions per unit of oxygen-defect formation are reduced to Ce^{3+}. The cluster charge, -12, confirms that two of the nine Ce cations have a charge of $+3$ and the other seven have a charge of $+4$.

Several kinds of interaction between 1,3-butanediol and the $CeO_2(111)$ surface were confirmed, as shown in Fig. 7. We can identify whether the PIO has an in-phase or an out-of-phase interaction between 1,3-butanediol and the $(Ce_9O_{36}H_{26})^{12-}$ cluster by determining the OP of each PIO; positive OP means in-phase interaction, whereas negative OP means out-of-phase interaction. Thus, PIOs 1–4 indicate that 1,3-butanediol is anchored on the oxygen-defect site of the $CeO_2(111)$ surface via the interaction between two O atoms and Ce cations (Table 3). In PIO-3, out-of-phase interaction between O^1 and C^1 is observed in 1,3-butanediol; that is, the $2p_y$ orbital of the O^1 atom interacts with the opposite phase of the $2p_y$ orbital of the C^1 atom (Fig. 7c; Table 3, row 6). PIO-5 and PIO-6 also show the out-of-phase interaction between $H^{2\alpha}$ and C^2 atoms. The 1s orbital of $H^{2\alpha}$ interacts with the opposite phase of the 2s orbital of C^2 atom in PIO-5 (Figs. 7d and 7f; Table 3, row 10) and PIO-6 (Fig. 7e; Table 3, row 12). These interactions result in the activation of C^1–O^1 and C^2–$H^{2\alpha}$ bonds and an increase in bond length (Table 1). Such interactions are hardly observed between O^3 and C^3, probably because of the large distance between O^3 and Ce^3, which causes inefficient overlap of the orbitals between O^3 and Ce^3 atoms.

In our previous studies, we proposed that O^1, $H^{2\alpha}$, and O^3 atoms coordinate to three Ce cations exposed at the oxygen-defect site of the $CeO_2(111)$ surface [2,4]. The present results show that 1,3-butanediol is anchored on the surface via the interaction between its two O atoms and the Ce cations, whereas its $H^{2\alpha}$ atom does not coordinate with the Ce cation. Another difference in the present study is the out-of-phase interaction seen between O and C atoms (PIO-3), which was not observed in the previous study. We speculate that these differences are related to the different adsorption models used. We previously used the speculative adsorption model of 1,3-butanediol at an oxygen-defect site of the $CeO_2(111)$ surface. Although the adsorption models are similar, PIO calculations are sensitive to the slight differences between the models. Hence, in this study, we could not confirm the orbital interaction that corresponds to the coordination of $H^{2\alpha}$–Ce^2 [4]; rather, we observed the out-of-phase interaction between O and C atoms in 1,3-butanediol.

4.5. Adsorption of 1,3-butanediol on stoichiometric $CeO_2(111)$ surface

The oxygen-defect site on the $CeO_2(111)$ surface is considered to act as an active center for the dehydration of 1,3-diol to form unsaturated alcohols. However, as far as we know, the adsorption of 1,3-diol on a stoichiometric $CeO_2(111)$ surface has not been investigated. Consequently, we performed DFT calculations to confirm the adsorption of 1,3-butanediol on a stoichiometric $CeO_2(111)$ surface (Fig. 8). As shown in Table 1, the C^1–O^1 and C^3–O^3 bond lengths increased after adsorption on the oxygen-defect site (Structure 2), whereas the C^3–O^3 bond length decreased after adsorption on the stoichiometric surface (Structure 3). This means that the O–C bond cleavage does not occur on the stoichiometric surface. Furthermore, the adsorption energy of Structure 3 is smaller than that of Structure 2 by 20.0 kJ mol^{-1}. This indicates that the dehydration proceeds preferentially at the oxygen-defect site.

4.6. Adsorption of 1- and 2-butanol on the $CeO_2(111)$ surface

Finally, we discuss the adsorption of 1- and 2-butanol on the oxygen-defected and stoichiometric $CeO_2(111)$ surfaces. The adsorption energies of butanols are much lower than those of 1,3-butanediol on the $CeO_2(111)$ surface (Table 2). Fig. 10 illustrates the difference in adsorption structure between 1,3-diols and mono-alcohols. Butanol adsorbs on the oxygen-defect

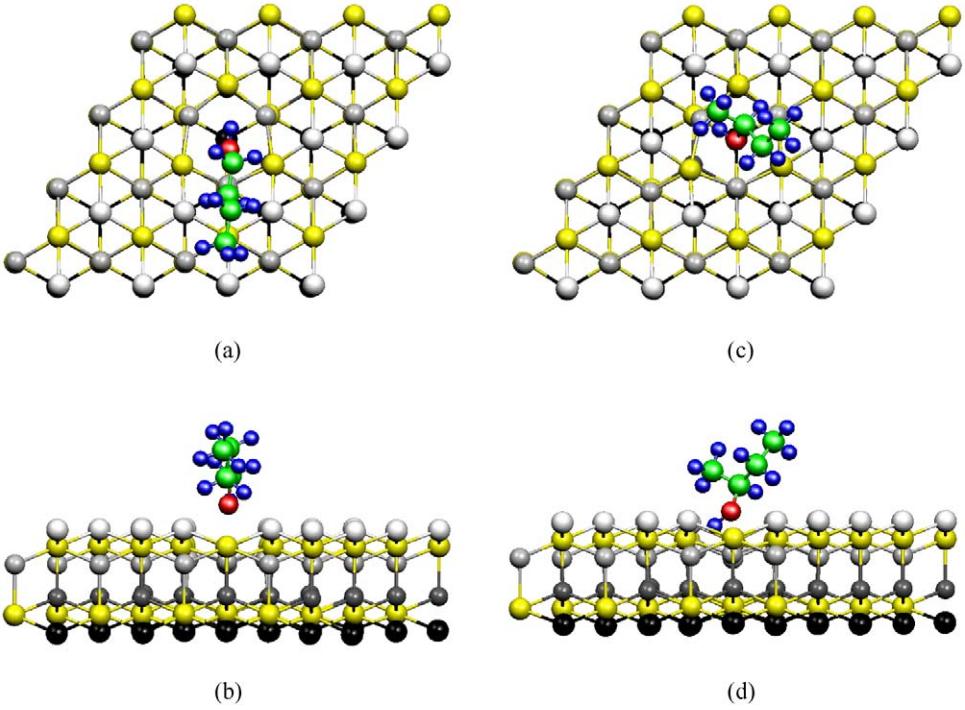

Fig. 9. Adsorption structures of 1- and 2-butanol at oxygen-defect site of $CeO_2(111)$ surface optimized by DFT calculations. Adsorption of 1-butanol (a) top view and (b) side view, and that of 2-butanol (c) top view and (d) side view. The O atom, represented by X in Fig. 2, is removed in the side view.

Table 4
Catalytic reaction of 1,3-butanediol over CeO_2 with different crystallite sizes

D[a,b] (nm)	Conversion[a,c] (%)	Selectivity (mol%)[a,c]			Formation rate[d]	
		3B2O	t2B1O	c2B1O	mmol h^{-1} g^{-1}	mmol h^{-1} m^{-2}
6.0	35.4	37.2	24.7	1.8	49.8	0.35
11.4	37.1	47.3	32.6	2.1	67.2	0.91
20.1	33.3	53.0	35.0	2.2	66.3	1.58
36.7	28.0	57.6	36.9	1.9	59.6	2.59
65.0	21.2	58.1	37.8	1.9	45.8	3.52

[a] Data are cited from Ref. [3].
[b] Particle size of CeO_2, D, is calculated with the equation, $D = 6/(d \times SA)$, where SA and d are the specific surface area and the density of CeO_2, $d = 7.1\ g\,cm^{-3}$, respectively.
[c] The reaction conditions are as follows: reaction temperature, 325 °C; catalyst weight, 0.5 g; liquid feed rate, 10 $cm^3\,h^{-1}$; N_2 gas flow rate, 1800 $cm^3\,h^{-1}$. 3B2O, 3-buten-2-ol; t2B1O, *trans*-2-buten-1-ol; c2B1O, *cis*-2-buten-1-ol.
[d] Formation rate of unsaturated alcohols is calculated from conversion–selectivity data.

site to fill the site with the O atom of its OH group, and the β-H atom of butanol seems not to interact with Ce cations. In contrast, the β-H atom ($H^{2\alpha}$ atom) and the two OH groups of 1,3-butanediol interact with Ce cations, as discussed in Section 4.4.

The difference in adsorption structure between mono-alcohols and 1,3-diols at the oxygen-defect site affects the difference in their reactivity; 1- and 2-butanol are less easily dehydrated than 1,3-butanediol over CeO_2 [2]. In Section 4.3, we stated that the oxygen-defect site would be the active center for the dehydration of 1,3-diols. In our previous study, we concluded that β-H elimination was the initial step in the dehydration of 1,3-diols [4]; the β-H atom in 1,3-butanediol was

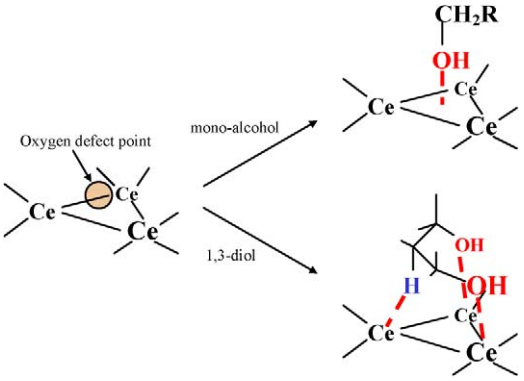

Fig. 10. Schematic image of the adsorption structures of 1,3-diols and mono-alcohols.

abstracted by a Ce cation. Actually, the dehydration of mono-alcohols occurs rarely, because the β-H atom cannot access Ce cations, and the mono-alcohols are dehydrogenated to form carbonyl compounds at higher temperatures [2]. Unsaturated mono-alcohols are not dehydrated and are selectively produced in the reaction of 1,3-diols due to the suppression of further dehydration to form dienes.

5. Conclusion

The adsorption of 1,3-butanediol on an oxygen-defected $CeO_2(111)$ surface was investigated using DFT and PIO calculations. Two optimized adsorption structures of 1,3-butanediol were obtained from different starting geometries by DFT calculations. Structure 2 (Fig. 4) was more stable than Structure 1 (Fig. 3), by 3.9 kJ mol^{-1}. Three bonds were activated by ad-

sorption: The C^1–O^1, C^2–$H^{2\alpha}$, and C^3–O^3 bond lengths in 1,3-butanediol were increased after adsorption in Structure 2.

PIO calculations indicated an in-phase interaction between the O atoms in 1,3-butanediol and Ce cations, indicating that 1,3-butanediol is anchored by the interaction between two O atoms and two Ce cations. The out-of-phase interactions between O^1 and C^1 and between $H^{2\alpha}$ and C^2, induced by the in-phase interactions between O^1 and Ce^1 and between $H^{2\alpha}$ and Ce^2, respectively, result in the elongation of the C^1–O^1 and C^2–$H^{2\alpha}$ bonds.

We also found that the adsorption energy of 1,3-butanediol on the stoichiometric $CeO_2(111)$ surface was substantially smaller (by 20.0 kJ mol^{-1}) than that at the oxygen-defect site. We speculate that 1,3-butanediol preferentially adsorbs on the oxygen-defect site of the $CeO_2(111)$ surface and is dehydrated at the defect site.

References

[1] S. Sato, R. Takahashi, S. Sodesawa, N. Honda, H. Shimizu, Catal. Commun. 4 (2003) 77–81.
[2] S. Sato, R. Takahashi, S. Sodesawa, N. Honda, J. Mol. Catal. A 221 (2004) 177–183.
[3] A. Igarashi, N. Ichikawa, S. Sato, R. Takahashi, T. Sodesawa, Appl. Catal. A 300 (2006) 50–57.
[4] N. Ichikawa, S. Sato, R. Takahashi, T. Sodesawa, J. Mol. Catal. A 231 (2005) 181–189.
[5] B. Delley, J. Chem. Phys. 92 (1990) 508–517.
[6] B. Delley, J. Chem. Phys. 113 (2000) 7756–7764.
[7] S.J. Vosko, L. Wilk, M. Nusair, Can. J. Phys. 58 (1980) 1200–1211.
[8] J.P. Perdew, K. Burke, M. Ernzerhof, Phys. Rev. Lett. 77 (1996) 3865–3868.
[9] H.J. Monkhorst, J.D. Pack, Phys. Rev. B 13 (1976) 5188–5192.
[10] C.R.A. Catlow, L. Ackermann, R.G. Bell, F. Cora, D.H. Gay, M.A. Nygren, J.C. Pereira, G. Sastre, B. Slater, P.E. Sinclair, Faraday Discuss. 106 (1997) 1–40.
[11] MOLEKEL 4.0, P. Flükiger, H.P. Lüthi, S. Portmann, J. Weber, Swiss Center for Scientific Computing, Manno (Switzerland), 2000.
[12] H. Fujimoto, N. Koga, K. Fukui, J. Am. Chem. Soc. 103 (1981) 7452–7457.
[13] H. Fujimoto, Acc. Chem. Res. 20 (1987) 448–453.
[14] T. Motoki, A. Shiga, J. Comput. Chem. 25 (2004) 106–111.
[15] A. Shiga, H. Kawamura-Hirabayashi, T. Sasaki, J. Mol. Catal. 87 (1994) 243–261.
[16] A. Shiga, H. Kawamura-Hirabayashi, T. Sasaki, J. Mol. Catal. A 98 (1995) 15–24.
[17] A. Shiga, J. Mol. Catal. A 146 (1999) 325–334.
[18] M. Ishida, T. Suzuki, H. Ichihashi, A. Shiga, Catal. Today 87 (2003) 187–194.
[19] G. Burns, J. Chem. Phys. 41 (1964) 1521–1522.
[20] P. Pyykkö, L.L. Lohr Jr., Inorg. Chem. 20 (1981) 1950–1959.
[21] Z.L. Wang, X. Feng, J. Phys. Chem. B 107 (2003) 13563–13566.
[22] S. Tsunekawa, T. Fukuda, A. Kasuya, Surf. Sci. 457 (2000) L437–L440.
[23] I. Kosacki, T. Suzuki, H.U. Anderson, P. Colomban, Solid State Ionics 149 (2002) 99–105.
[24] H. Nörenberg, G.A.D. Briggs, Surf. Sci. 402–404 (1998) 734–737.
[25] H. Nörenberg, G.A.D. Briggs, Surf. Sci. 424 (1999) L352–L355.
[26] K. Fukui, Y. Namai, Y. Iwasawa, Appl. Surf. Sci. 188 (2002) 252–256.
[27] Y. Namai, K. Fukui, Y. Iwasawa, Catal. Today 85 (2003) 79–91.
[28] F. Esch, S. Fabris, L. Zhou, T. Montini, C. Africh, P. Fornasiero, G. Comelli, R. Rosei, Science 309 (2005) 752–755.
[29] M. Cococcioni, S. de Gironcoli, Phys. Rev. B 71 (2005) 035105.
[30] S. Fabris, S. de Gironcoli, S. Baroni, G. Vicario, G. Balducci, Phys. Rev. B 71 (2005) 041102.